Iranian Journal of Oil & Gas Science and Technology, Vol. 2 (2013), No. 2, pp. 34-49
http://ijogst.put.ac.ir

Gas-liquid Relative Permeability Estimation in 2D Porous Media by Lattice Boltzmann Method: Low Viscosity Ratio 2D LBM Relative Permeability

S. Mahmoudi[1], A. Hashemi[1*], and Sh. Kord[2]

[1] Department of Petroleum Engineering, Petroleum University of Technology, Ahwaz, Iran
[2] Department of Reservoir Engineering, National Iranian South Oil Company, Ahwaz, Iran

Abstract

This work is a primary achievement in studying the CO_2 and N_2–oil systems. To predict gas-liquid relative permeability curves, a Shan-Chen type multicomponent multiphase lattice Boltzmann model for two-phase flow through 2D porous media is developed. Periodic and bounce back boundary conditions are applied to the model with the Guo scheme for the external body force (i.e., the pressure gradient). The influence of relationship between cohesion and adsorption parameters and the interfacial tension values in Young's equation, pore structure (micro scan image derived porous media response is compared with corresponding porosity and permeability ideal sphere pack structure), and saturation distribution on relative permeability curves are studied with the aim to achieve the realistic stable condition for the simulation of gas-liquid systems with a low viscosity ratio.

Keywords: Relative Permeability, Lattice Boltzmann Model, Guo Scheme, Micro Scan Image, Gas Liquid System

1. Introduction

As a matter of concern, the relative permeability curves play an important role in the estimation of the final oil recovery in any simulation studies and subsequent decision making in reservoir engineering. The relative permeability concept is based on a modification of Darcy's law that defines the permeability of a 100% saturated medium under laminar steady state single-phase flow conditions.

In immiscible flow through porous media, the wetting fluid moves next to the solid surface and the non-wetting phase flows in the central part of the pore space surrounded by the wetting fluid. A modification of Darcy's law to account the momentum transfer across the interfaces leads to defining an apparent relative permeability $k_{r,i}$, which is a function of wetting phase saturation, S_w, capillary number, Ca, and viscosity ratio M (Yiotis et al., 2007), and is defined as "Effective permeability divided by permeability to non-wetting phase at $S_{w\,(min)}$." (Archer and Wall, 1986).

$$\tilde{u}_i = -\frac{k k_{r,i,app}(S_w, Ca, M, \nabla P_j)}{\mu_i} \nabla P_i \qquad (1)$$

Precise determinations of gas-oil relative permeability data are expensive and difficult, although there are several factors affecting the accuracy. An alternative approach to this aim is the use of pore-scale modeling including both pore network (PNM) and lattice Boltzmann modeling (LBM). The lattice Boltzmann advantage for porous media lies in its ability to incorporate complex boundary conditions relative to continuum modeling approaches and an excellent ability to simulate interfaces between

* Corresponding Author:
Email: a.hashemi@put.ac.ir

different fluids.

Several LB models have been applied to investigate multiphase flow through porous media; “color method” by Gunstensen et al., (1991), “potential method” by Shan and Chen, (1993), “free-energy model” by Swift et al., (1995), and ”incompressible-index model” by He et al., (1999) are some popular ones.

The simulation of two-phase flow in porous media (Pan et al., 2004; Li et al., 2005) and more complex two-phase processes such as viscous fingering in Hele–Shaw cells (Grosfils et al., 2004) and the dynamics of liquid bubbles under gravity (Lee and Lin, 2005) among others are some of recent applications of LBM. These works demonstrate the LBM remarkable ability for the computational modeling of multiphase flow problems (Yiotis et al., 2007).

The validity of Darcy’s law-based relative permeability concepts has been the objective of most applications of multiphase lattice gas and LB methods to porous media but for multicomponent oil/water-like systems (Sukop and Or, 2004). Some recent efforts to study the gas liquid systems are the works by Yiotis et al., (2007) who carried out a lattice Boltzmann study of viscous coupling effects in immiscible two-phase flow in porous media based on the single-component multiphase model of He et al., (1999) assuming that the pressure of non-ideal fluids is described by the Carnahan–Starling EOS, the work of Huang et al., (2008) who investigated the viscous coupling effects for two-phase flow in porous media based on Shan-and-Chen-type multiphase lattice Boltzmann, and Huang and Lu (2009) who studied the relative permeability and coupling effects in steady-state gas-liquid flow in porous media based on Shan-and-Chen-type multiphase lattice Boltzmann method. The last two works have used the single component multiphase model (like water and its vapor) along with the R-K equation of state to model gas-liquid systems with a high density ratio. They have used the original Shan-Chen scheme for the incorporation of body forces and investigated the co- and counter-current steady-state two-phase flow patterns and relative permeability as a function of wetting saturation for different capillary numbers, wettabilities, and viscosity ratios.

In this paper, we have studied the apparent relative permeabilities of gas-liquid systems based on LB model by Shan and Chen but using the multicomponent multiphase model (which is useful for the simulation of different fluid pairs with essentially different kinematic viscosities) and the Guo scheme for body force (the best representative of continuity and momentum equations on the macroscopic scale). We have also investigated the relationship between cohesion and adsorption parameters and the interfacial tension values in Young's equation and the influence of pore structure and saturation distribution on relative permeability curves.

An outline of the paper goes as follows. After a brief review of the theory of the LB method, the validating predictions of the model for fluid flow in a few simple geometries are reviewed. Then, gas-liquid relative permeability curves are calculated as a function of wetting fluid saturation, M, for a specific Ca. The influence of wettability parameters (relationship between adsorption and cohesion terms), pore structure, and initial saturation distribution on these curves are discussed. The concluding remarks come afterward.

2. LB method

2.1. Basics of LBM

In this method, in 2D models the domain is divided into regular lattices with the same spacing in both x- and y-directions, and, at each lattice site, a distribution function $f_m^{\sigma}(x, y, t)$ is defined which denotes the expected number of particles of fluid σ at that site (x, y) in the direction of m with a velocity of e_m. During each time step, the streaming and collisions of these particles at that direction are performed through the Boltzmann equation:

$$\frac{\partial f_i}{\partial t} + e_i \frac{\partial f_i}{\partial x} = \frac{f_i - f_i^{eq}}{\tau} \quad (2)$$

Particle positions are confined to the nodes of the lattice. Changes in momentum and magnitudes and varying particle mass are reduced to 8 directions, 3 magnitudes, and a single particle mass (Sukop and Thorne, 2007). The macroscopic fluid density is the sum of directional densities:

$$\rho = \sum_{\alpha=1}^{9} f_\alpha \quad (3)$$

The macroscopic velocity u is an average of the microscopic velocities em weighted by the directional densities fm:

$$u = \frac{1}{\rho} \sum_{\alpha=1}^{9} f_\alpha e_\alpha \quad (4)$$

The fluid kinematic viscosity is defined as

$$\nu = \frac{1}{6}(\tau - 0.5) \quad (5)$$

where, τ is the relaxation time, which in BGK (single relaxation time) model relaxes the distribution function towards local equilibrium. Streaming and collision read:

$$f_\alpha(x + e_\alpha \Delta t, t + \Delta t) = f_\alpha(x, t) - \frac{f_\alpha(x,t) - {f_\alpha}^{eq}(x,t)}{\tau} \quad (6)$$

$${f_\alpha}^{eq}(x) = w_\alpha \rho(x) \left[1 + 3\frac{e_\alpha . u^{eq}}{c^2} + 9\frac{(e_\alpha . u^{eq})^2}{c^4} - \frac{3}{2}\frac{{u^{eq}}^2}{c^2}\right] \quad (7)$$

$$u^{eq} = u + \Delta u = u + \frac{\tau F}{\rho} \quad (8)$$

$$w_1 = \frac{4}{9};\ w_{2345} = \frac{1}{9};\ w_{6789} = \frac{1}{36}$$

where, F is the applied body force.

2.2. Shan-Chen potentials for multiphase systems

Equilibrium velocity for fluid σ is defined as:

$${\vec{u}_\sigma}^{eq} = \vec{u}' + \frac{\tau_\sigma \vec{F}}{\rho_\sigma} \quad (8)$$

where, F and u' are the total force and composite velocity respectively. $F = F_{\text{inter particle}} + F_{\text{adsorption}} + F_{\text{external}}$

$$\vec{u}' = \frac{\sum_\sigma \sum_{\alpha=1}^{9} \frac{f_\alpha^\sigma \vec{e}_\alpha}{\tau_\sigma}}{\sum_\sigma \frac{\rho_\sigma}{\tau_\sigma}} \quad (9)$$

Inter-particle and adsorption interaction forces are calculated based on the nearest neighboring nodes with the following form:

$$F_{int}(x,t) = -G_c \psi_\sigma(x,t) \sum_{\alpha=1}^{9} w_\alpha \psi_{\bar{\sigma}}(x + e_\alpha \Delta t, t) e_\alpha \quad (10)$$

$$F_{ads}(x,t) = -G_{ads} \psi(x,t) \sum_{\alpha=1}^{9} w_\alpha S(x + e_\alpha \Delta t) e_\alpha \quad (11)$$

where, σ and $\bar{\sigma}$ denote two different fluids; G_c and G_{ads} are used to control the IFT and the surface wettability. Due to the nature of the interaction between two fluids, smaller values of G_c lead to diffused interfaces, whereas larger values lead to sharp interfaces and purer components. However, the simulation suffers from numerical instability after some critical values. The sign of these parameters

indicate the repulsion or attraction nature of the forces and their absolute value can be adjusted to model the desired IFT and contact angles. S in Equation 12 is an indicator of solid sites (1) or pore sites (0). For the EOS proposed by Shan and Chen, the potential function is given by:

$$\psi(\rho) = \rho_0 \left[1 - \exp\left(-\frac{\rho}{\rho_0}\right)\right] \quad (12)$$

The pressure at position x can be determined from the fluid densities as reads (Huang et al., 2007)

$$P(x) = \frac{1}{3}\left(\rho_1(x) + \rho_2(x)\right) + \frac{1}{3} G\psi_1(x)\psi_2(x) \quad (13)$$

2.3. Incorporation of external body force

In this section, some widely used methods of adding external force to LBM will be reviewed; they are three schemes I, II, and III (Mohammad and Kuzmin, 2010).

The force term added to the collision process as $F_i = 3w_i F e_i$ and the velocity field is not shifted. As used by Shan and Chen, the velocity field is shifted as $u(x,t) = \frac{1}{\rho}\sum_{i=1}^{9} f_i(x,t)e_i + \frac{F\tau}{\rho}$ which is based on Newton's second law. For this scheme no force term is added to the collision process.

Guo scheme: $F_i = w_i\left(1 - \frac{1}{2\tau}\right)[3(e_i - u) + 9e_i(e_i.u)].F$. This term needs to be added into the collision process and the velocity also needs to be shifted as $u^{eq} = \frac{1}{\rho}\sum_{i=1}^{9} f_i e_i + \frac{F\Delta t}{2\rho}$.

Herein, we incorporate the Guo scheme since Guo et al. (2002) analysis showed the method suggested by them was the best representative of continuity and momentum equations on the macroscopic scale, i.e., the Navier-Stokes equation.

2.4. Boundary conditions

For simulating the non-slip boundary condition (the usual practice in classic fluid dynamics) at solid nodes, the "bounce-back" method is applied. Herein, we use the "mid-plane" bounce back scheme and fully periodic boundaries have been applied at the non-solid boundaries of the domain to get an infinite domain of fluid. In periodic boundary conditions, nodes on the opposite boundary are simply considered as the neighboring points of the boundary nodes.

3. Results and discussions

The conventional procedure for verifying LB models is the primary bubble and contact angle tests proceeding by the channel flow simulation for the investigation of poiseuille flow pattern as has been used in the works of Huang et al., (2007; 2008; 2011), Sukop and Or (2004), Sukop and Thorne (2007), Ghassemi and Pak (2011), and Yiotis et al. (2007) among others. For the simulation of relative permeability curves, we do need to simulate single phase flow too. A simple verification of single-phase models is the model ability to predict the absolute permeability of a simple porous media like ideal sphere packs.

3.1. Permeability to sphere pack porous media

A simple and primary benchmark to the model is the ability to predict Darcy's permeability of a simple porous media that is sphere pack model. To this end, a sand pack is considered as the sphere pack which should be applied to the model through Kozeny-Carman correlation. The sand pack was prepared at the reservoir rocks laboratory of Petroleum University of Technology with a length of 1 m and a diameter of 5 cm. The permeability to water was measured to be 1.44 D and the porosity to be 26%. These properties along with the correlation $k = \phi^3 d^2/(180(1-\phi)^2)$ (Kaviany, 1995) yield

grain sizes of 0.09 mm. This grain size serves as the characteristic length to be applied in the model. 26% porosity implies that rhombohedral-pack spheres model should be implemented. This structure is illustrated in Figure 1. The 2D structure was introduced to the model by a bitted-map digital image constructed by the indicators of solid sites (1) and pore sites (0).

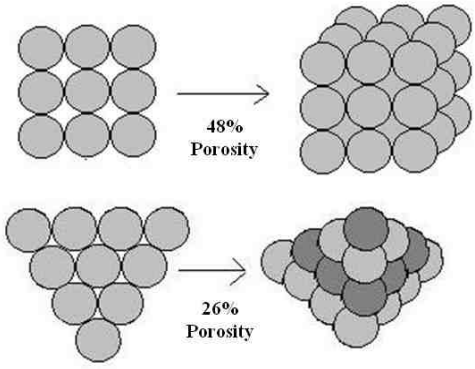

Figure 1
A schematic of regular cubic and rhombohedral pack spheres

For Darcy flow, one may obtain:

$$k = -\frac{U\mu}{dp/dx} \tag{14}$$

where, U is the superficial fluid speed averaged across an outlet face of the medium (including solids); μ is the dynamic viscosity; dP/dx stands for the pressure gradient along the x-direction. To relate the permeability to units measured in the LB simulation, we apply a force balance:

$$xBody.x^3 = (P_{in.} - P_{out}).x^2 = -\left(\frac{dP}{dx}\right)x^3 \rightarrow xBody = -\left(\frac{dP}{dx}\right) \tag{15}$$

where, x is the side of the simulation cell (in lattice units) and xBody represents the body force applied in the x-direction per unit volume in the LB simulation Therefore:

$$k = -\frac{U\nu\rho}{xBody} \tag{16}$$

For the characteristic length considered here, every 615 lattice unit (lu) represents 1 mm in physical domain; thus, for the porous medium with a sphere diameter of 550 lu, we have $550/615 = 0.09$. To convert the LB permeability to physical permeability, we perform $(0.001\text{m}/615\text{ lu})^2 \times k_{LB}$.
Reynolds number was also maintained low to ensure the applicability of Darcy's law; the maximum lattice velocity of 0.007 lu/ts with a kinematic viscosity of 0.167 lu^2/ts and a pore diameter of 20 lu result $Re = Ud/\nu = 0.84$.
As mentioned in the work of Huang et al., (2011), for single-phase flow, the permeability of the porous medium is slightly dependent on τ when the BGK model is used for the collision term; hence the fluid fluxes can be calculated for the specified Gc and τ. The simulation results show good agreement with Kozeny correlation with less than 10% error as the resolution increases. It can be seen in Figure 2 that increasing the resolution stabilizes the resulted permeability to about 1.6 D with 10% offset from the predicted value of Kozeny correlation. However, the obtained precision is acceptable relative to the difference exists between various correlations. The estimated lower LBM permeability at a lower resolution is rooted in the roughness effect of digital images in the representation of the sphere surface with a finite number of solid sites; this causes the spheres to appear somewhat jagged and results in a kind of barrier to flow.

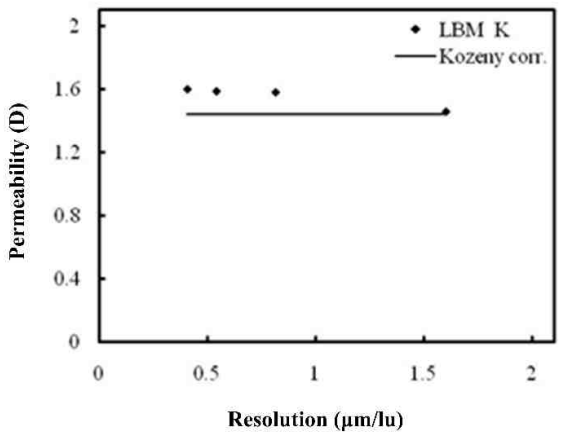

Figure 2
Kozeny-Carman and LBM permeability

3.2. Simulations of IFT and wettability

When the Shan Chen lattice Boltzmann model is applied, a necessary part of analyses is the bubble test; this is because, in SC model, the interfacial tension is not a direct input and the strength of surface tension is controlled by the parameter Gc. The same reason stands for wetting characteristic of a solid controlled by the parameter Gads through contact angle test.
In multicomponent LB models, the bubble tests check the ability of the model in relating the pressure difference (Δp), radius of curvature (R), and interfacial tension (γ) when a bubble of one fluid is immersed in another fluid as follows:

$$\Delta p = \frac{\gamma}{R} \tag{17}$$

In this test, various initial bubbles of less viscous fluid is placed in a domain with a size of 150 lu × 150 lu for two sets of density values (Figures 3 and 4).

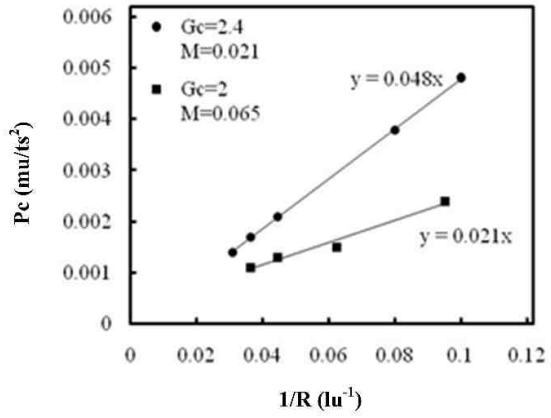

Figure 3
IFT simulation for small fluid densities

The contact angle test not only demonstrates the ability to model different wetting behavior, also verifies the assumption of direct relationship between cohesion and adsorption parameters and the interfacial tension values in Young's equation (Equation 19).

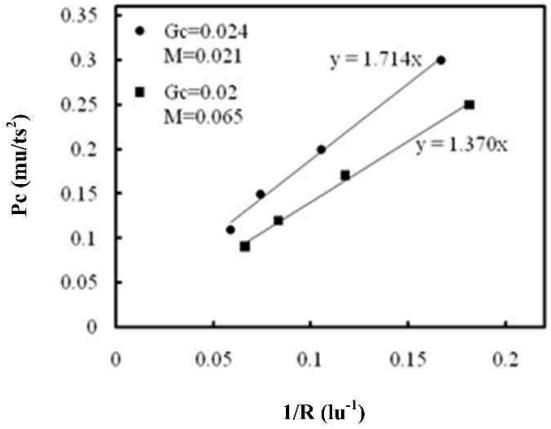

Figure 4
IFT simulation for 40-fold larger fluid densities

The following equations are applied to calculate the contact angles, with the parameters R, L, and H used for the drop radius, drop base, and drop height respectively as demonstrated in Figure 5.

$$\gamma \cos\theta = (\gamma_{s2} - \gamma_{s1}) \quad (19)$$

$$\cos\theta = \frac{G_{ads2} - G_{ads1}}{G_c} \quad (18)$$

$$R = \frac{4H^2 + L^2}{8H} \quad (19)$$

$$\tan\theta = \frac{L}{2(R-H)} \quad (20)$$

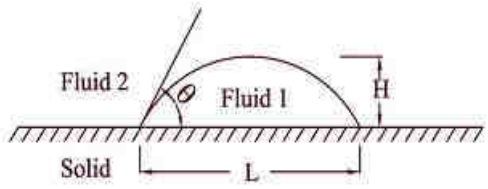

Figure 5
Contact angle definition

In contact angle tests, a drop with a diameter of 30 lu is placed in a domain with a size of 120 lu × 150 lu. According to Huang et al., (2007), when Gcρi>2, the compressibility effect of LBM increases; this causes some deviation from the direct relationship between cohesion and adsorption parameters and the interfacial tension values in Young's equation. Based on our simulations for a specific density ratio, the choice of the density values itself is a cause of distortion from the linear trend of contact angles versus the drop adsorption Gads1 (Gcρi<2). This factor constrains the proper possible choices of the cohesion parameter in a way that if larger density values are selected, smaller values of Gc must be assigned, and hence the adhesion parameters will become several times larger than cohesion, which subsequently violates the cosine definition in Equation 19. But an exciting effect of large density values and low cohesion parameter is that a larger IFT—which is preferred in flow simulations—is obtained as shown in Figures 3 and 4. For small density values and Gcρi>2, an S-shape relationship, and for Gcρi<2, a linear relationship between the contact angle and the adhesion parameter was detected as shown in Figures 6 and 7.

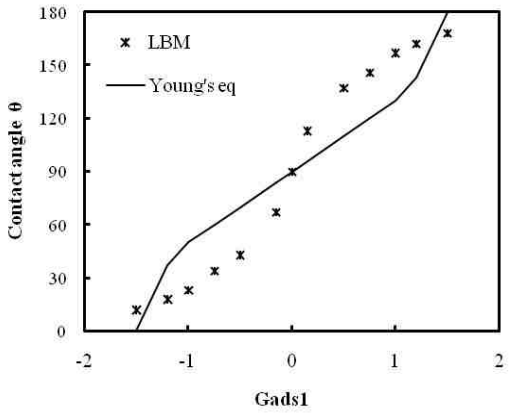

Figure 6
Calculated contact angles as a function of drop adsorption parameter, G_{ads1}, for $G_c\rho_i>2$

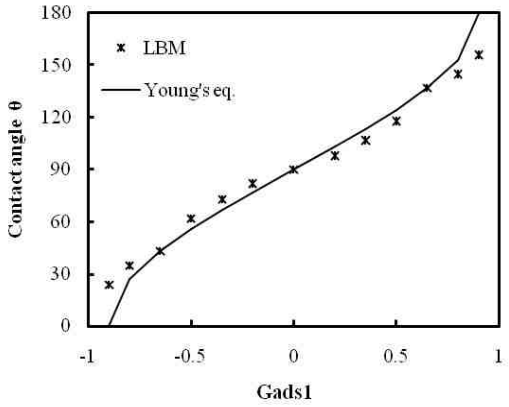

Figure 7
Calculated contact angles as a function of drop adsorption parameter, G_{ads1}, for $G_c\rho_i<2$

3.3. Two-phase flow in a 2D channel

a. Flow characteristics

To check the model ability to simulate multiphase flow problems, we investigate the poiseuille pattern in a 2D channel. Owing to periodicity, a 121 lu × 11 lu domain is considered to reduce the computational cost and the rather thick interface (6-8 lu) effect in SC model. By the analytical solution of poiseuille flow in a channel, the corresponding relative permeability for wetting and non-wetting phases are given by (Yiotis et al., 2007):

$$k_{r,w} = \frac{1}{2}{S_w}^2(3 - S_w) \tag{21}$$

$$k_{r,nw} = S_{nw}\left[\frac{3}{2}M + {S_{nw}}^2\left(1 - \frac{3}{2}M\right)\right] \tag{22}$$

In immiscible flow through porous media, the wetting fluid moves next to the solid surface and the non-wetting phase flows in the central part of the pore space surrounded by the wetting fluid. Sw is defined as $S_w = 1 - a/b$. According to Figure 8, LBM relative permeability is calculated at outlet face by the ratio of the cumulative flux of one fluid and the fluid flux when only that fluid exists in the domain. This method is applicable when Darcy's law conditions are satisfied; in other words, when

low Reynolds number and steady state (constant saturation) conditions are reached. The viscosity ratio and capillary number are defined as $M = \frac{\mu_{nw}}{\mu_w} = \frac{\nu_{nw}\rho_{nw}}{\nu_w\rho_w}$ and $Ca = \frac{\text{viscous force}}{\text{capillary force}} = \frac{F_{ext}}{\sigma}$ respectively. Ca can be regarded as the ratio of the body forces to the interfacial forces (Rothman, and Keller, 1988). In this study, F_{ext} is a uniform steady body force. The whole fluid velocity u is defined as $u = u' + \frac{F}{2\rho}$ where $\rho = \sum_\sigma \rho_\sigma$ and $\nu = \frac{1}{6}\left(\sum_\sigma x_\sigma \tau_\sigma - \frac{1}{2}\right)$; $x_\sigma = \rho_\sigma/\rho$ (Shan and Doolen, 1996).

These simulations are performed with tau values of 0.75 and 1.17, Gc = 3 and Gads = 1.5. The IFT and contact angle values are calculated as σ = 0.042 and θ = 9°; F_{ext} was equal to 0.0001 and thus $Ca = \frac{0.0001}{0.042} = 2.4 \times 10^{-3}$.

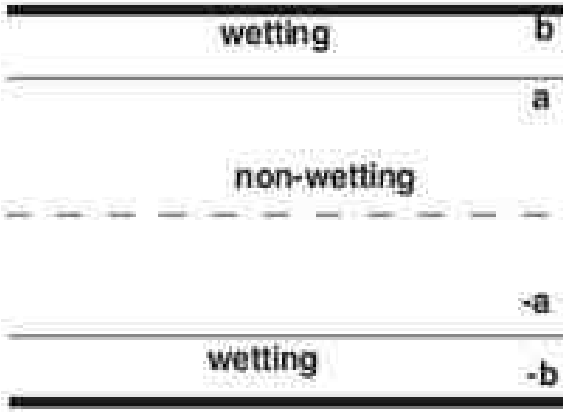

Figure 8
A schematic of two-phase Poiseuille flow in channel

b. Relative permeability for different M's

In a situation where the more viscous fluid is the wetting phase, the relative permeability of wetting and non-wetting fluids obeys the conventional pattern with the non-wetting relative permeability greater in magnitude. Figure 9 shows the analytical and simulation results. The velocity profile is also shown in Figure 10.

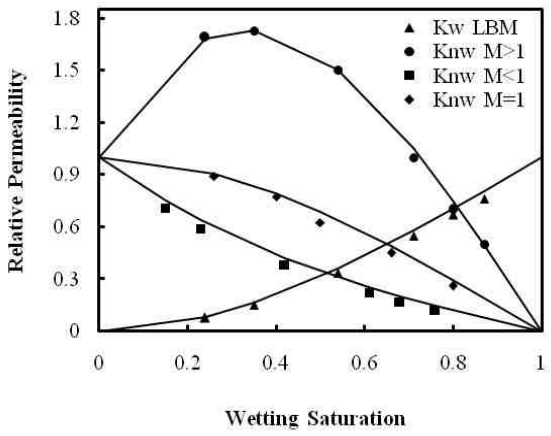

Figure 9
Comparison of LB modeling results and analytical solution for variation of relative permeabilities with respect to saturation ratio in two-phase Poiseuille flow

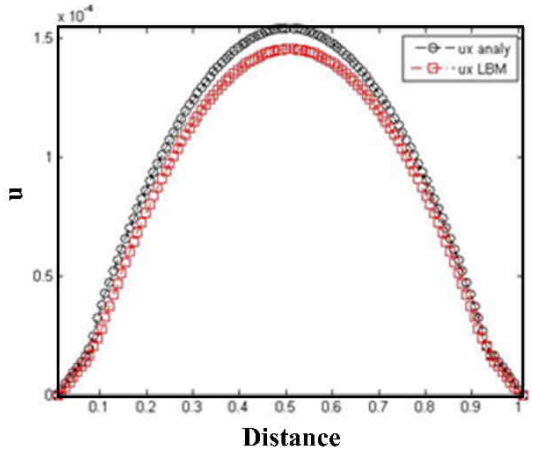

Figure 10
Velocity profile in the channel; comparison of LB modeling results and analytical solution of poiseuille flow

Since the relative permeability of wetting fluid is not a function of viscosity ratio when the viscosity of the wetting phase is less than that of non-wetting, no change will be made on its curve; however, the non-wetting fluid experience a lubricating effect during the flow and show a relative permeability greater than unity. Good agreement between analytical and simulation results are observed.

3.4. Two phase flow through porous media

So far, we have presented the verifying predictions of the developed SC model where the applied viscosity ratios were far from gas-liquid systems. In this section, the relative permeability curves for gas-liquid systems are calculated as a function of wetting saturation, Sw, viscosity ratio, M, and specified capillary number, Ca. All the simulations are assumed to reach steady state after 40000 time steps. Micro scan image derived porous media response is compared with corresponding porosity and permeability ideal sphere pack structure. The micro model has been engineered at Schlumberger Cambridge Research, based on a thin section of a 3D Berea sand stone rock sample with 22% porosity (Boek and Venturoli, 2010). Owing to our limitations in computing hardware, we used a piece of the micro model with a size of 569 μm × 891 μm, and due to the nature of periodic boundary conditions, we reproduced a symmetric image relative to x-y axes which had a porosity of 33%. For this low porosity and rather large domain size, we would need a powerful computing hardware; therefore, a more simplified image was derived from the symmetric image and compared with ideal sphere pack model with the pore throats of at least 20 lu (Figures 11-13).

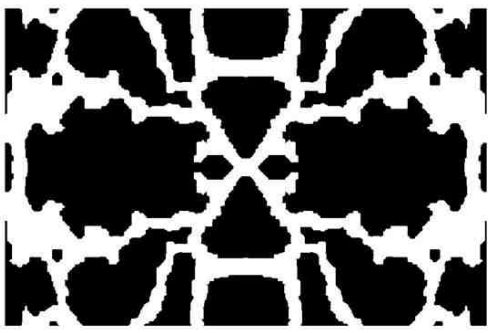

Figure 11
Micro model pore structure, 569 lu × 891 lu, 33% porosity

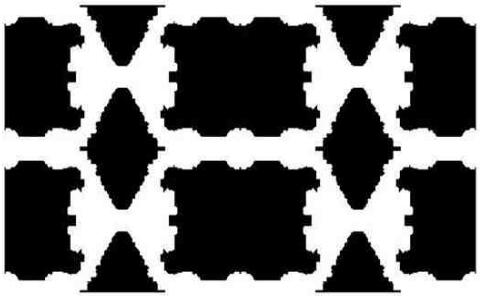

Figure 12
Simplified pore structure, 264 lu × 502 lu, 38% porosity

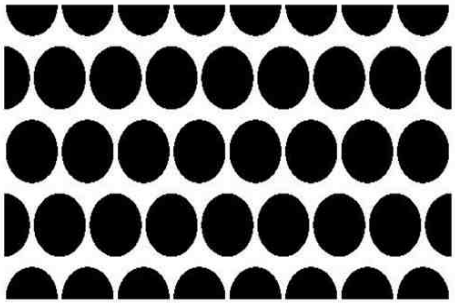

Figure 13
Ideal sphere pack, 262 lu × 484 lu, 38% porosity

a. Effect of viscosity

To simulate gas-liquid systems, fluids with a low viscosity ratio pair should be used. Because our objective for developing the SC model was to study the CO_2 and N_2–oil systems, we considered two viscosity ratios corresponding to the mentioned system viscosities at 2000 psi and 120 °F and found that smaller viscosities lead to a larger relative permeability; the reason was that low viscosity fluid had a higher mobility. These simulations were performed with the tau values 0.55 and 1.17 for the density ratio of 0.9 and M=0.065 and the tau values 0.55 and 1.8 for the density ratio of 0.6 and M=0.021. The Ca was set equal to 4.7×10^{-3}. These values imply that we should expect larger wetting phase relative permeability as shown in Figure 14.

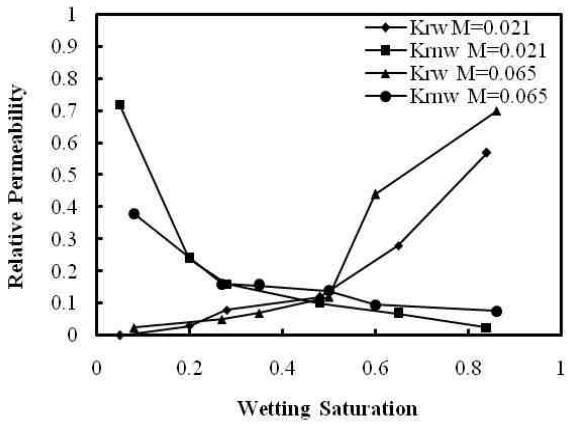

Figure 14
Effect of viscosity on relative permeability; for M=0.021 the wetting phase has a lower viscosity and a larger relative permeability

b. Effect of wettability

To explain the wettability effect on two-phase flow in porous media, we conduct two series of simulations with the mentioned conditions of adhesion and cohesion parameters according to the results presented in section 3.2,.

When the medium is neutrally or strongly wet, for both Gcρi>2 and Gcρi<2 same results were obtained; nevertheless, in the middle region, the relationship between contact angle and adhesion parameter affects the relative permeability curves of both wetting and non-wetting phases and can cause an increase or a reduction if direct relationship between cohesion and adsorption parameters and the interfacial tension values in Young's equation is assumed.

c. Initial saturation distribution

Two initialization methods for saturation distribution are considered, namely a random distribution and an injection-like initial saturation. The first case is suitable for a pair fluid with large density difference to gain stability and the second is more realistic in injection processes.

Initial saturation distribution affects the results in two ways: the required time to reach steady state condition and the end point relative permeabilities. In the case of random saturation distribution, the end point relative permeability occurred at higher saturations of the non-wetting fluid. Figure 15 portrays this effect.

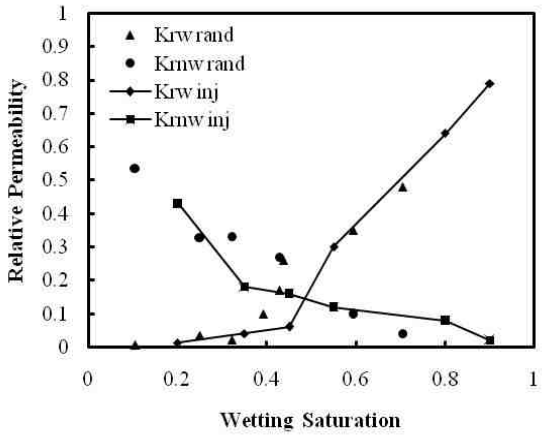

Figure 15

LB relative permeability for random and injection-like saturation distribution for M=0.065, σ=0.021, and Ca=4.7×10^{-3}; major effect is the end point relative permeability.

d. Effect of pore structure

Figures 16 and 17 illustrate the effect of pore structure on the relative permeability curves. In these figures, 1 and 2 identify the micro model and the ideal sphere pack model responses respectively. As illustrated, an increase in surface area reduced the non-wetting phase relative permeability but did not almost alter the wetting phase relative permeability. This finding could be implemented along with the saturation distribution effect to properly simulate real flow domains.

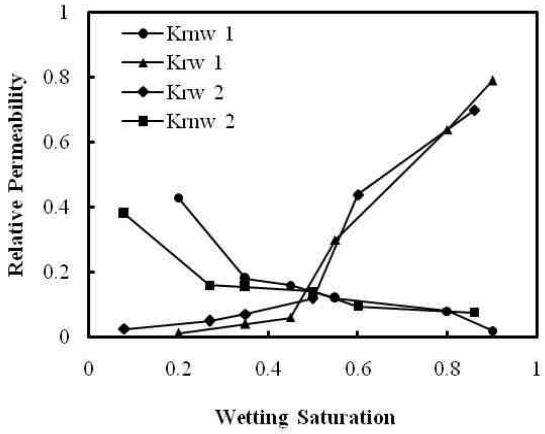

Figure 16
LB relative permeability for M= 0.065, σ=0.021, and Ca=4.7×10^{-3}; "1" indicates the micro model and "2" shows the sphere pack.

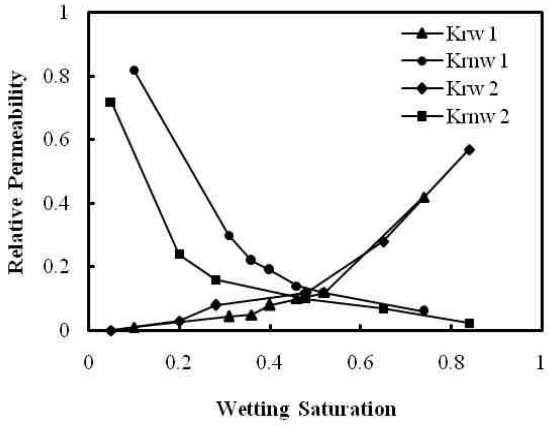

Figure 17
LB relative permeability for M=0.021, σ=0.048, and Ca=4.7×10^{-3}; "1" indicates the micro model and "2" shows the sphere pack.

4. Conclusions

In this paper, the multicomponent multiphase Shan-Chen type LBM was used to study the two-phase flow in porous media and to simulate gas-liquid relative permeability curves in a realistic pore structure. Relative permeability curves were calculated as a function of wetting saturation for different viscosity ratios, phase distribution patterns, wettability parameters (relationship between cohesion and adsorption parameters and the interfacial tension values in Young's equation), and pore structure. Because of very low viscosity ratios of gas-liquid systems, we considered two viscosity ratios and found that smaller viscosities lead to a larger relative permeability. When Gcρi>2, an S-shape relation and when Gcρi<2, a linear relationship between the contact angle and the adhesion parameter was detected which affected the relative permeability of both wetting and non-wetting phases and could increase or reduce their values. The effect of large density values (Gcρi<2) and low cohesion parameter was a larger IFT; nonetheless, the adhesion parameters became several times larger than cohesion term, which subsequently violated the cosine definition in Young's equation. Phase distribution affected the end point relative permeabilities. An increase in surface area reduced the non-wetting phase relative permeability but did not almost change the wetting phase relative permeability.

These results showed that SC-type multicomponent multiphase LB method was a powerful tool to investigate multiphase flow characteristics and could be considered as a substitution of experimental approaches.

Acknowledgements

We gratefully acknowledge the financial support for this research by the National Iranian South Oil Company (NISOC).

Nomenclature

BGK : Bhatnagar-Gross-Krook single relaxation time collision operator
Ca : Capillary number
IFT : Interfacial tension
LB : Lattice Boltzmann
LBM : Lattice Boltzmann modeling
SC : Shan and Chen
xBody : Body force in x direction

Scripts

ads : Adsorption
app : Apparent
c : Cohesion
d : Drop
e : Effective
eq : Equilibrium
ext : External
int : Inter particle
nw : Non-wet
r : Relative
w : Wet
α : Direction indicator
σ : Phase indicator

Latin Symbols

c : Basic lattice speed of particles (lu/ts)
d : Pore diameter (lu)
F : Body force (mu/(lu.ts^2))
F_{ext} : External body force (mu/(lu.ts^2))
F_{int} : Inter particle force (mu/(lu.ts^2))
F_{ads} : Adsorption force (mu/(lu.ts^2)
f_α : Directional density (local distribution function)
f_α^{eq} : Local equilibrium distribution function
G : Strength of interaction forces (1/ts)
G_{ads} : Strength of adsorption forces to control surface wettability (1/ts)
G_c : Strength of cohesion forces to control interfacial tension (1/ts)
k : Permeability (D)
k_r : Relative permeability (dimensionless)
k_e : Effective permeability (D)
$k_{r(app)}$: Apparent relative permeability (dimensionless)
L : Length (lu)
lu : Lattice unit
M : Viscosity ratio (dimensionless)
mu : Mass unit

P	: Pressure (mu/ts^2)
Pc	: Capillary Pressure (mu/ts^2)
S	: Saturation (fraction)
t	: Time (ts)
ts	: Time step
U	: Darcy velocity (m/s)
u	: Macroscopic velocity (lu/ts)
u′	: Composite (hole fluid) velocity (lu/ts)
w_α	: Directional weighting multiplier
x	: x-coordinate

Greek Symbols

Δ	: Delta operator
Ø	: Porosity
γ	: Young-Laplace interfacial tension (dyne/cm)
μ	: Dynamic viscosity (cp)
ν	: Kinematic viscosity (lu^2/ts)
θ	: Contact angle (degree)
ρ	: Average density (mu/lu^2)
σ	: Interfacial tension ($mu.lu/ts^2$)
τ	: Relaxation time (ts)
ψ	: Potential function (mu/lu^2)

References

Archer, J. S. and Wall, C. G., Petroleum Engineering, Principles and Practice, London, Graham and Trotman Ltd, 362 p., 1986.

Boek, E. S. and Venturoli, M., Lattice-Boltzmann Studies of Fluid Flow in Porous Media with Realistic Rock Geometries, Computers and Mathematics with Applications, Vol. 59, p. 2305-2314, 2010.

Ghassemi, A. and Pak, A., Numerical Study of Factors Influencing Relative Permeabilities of Two Immiscible Fluids Flowing through Porous Media Using Lattice Boltzmann Method, Journal of Petroleum Science and Engineering, Vol. 77, p. 135-145, 2011.

Grosfils, P., Boon, J. P., Chin, J., and Boek, E. D., Phil. Trans. R. Soc., 2nd Ed., Lond. A, Vol. 362, p. 1723-1734, 2004.

Gunstensen, A. K., Rothman, D. H., Zaleski, S., and Zanetti, G., Lattice Boltzmann Model of Immiscible Fluids, Physical Review A, Vol. 43, p. 4320-4327, 1991.

Guo, Z., Zheng, C., and Shi, B., Discrete lattice Effects on the Forcing Term in the Lattice Boltzmann Method, Physical Review E, Vol. 65, p. 463081-463086, 2002.

He, X., Chen, S., and Zhang, R., A lattice Boltzmann Scheme for Incompressible Multiphase Flow and its Application in Simulation of Rayleigh–Taylor Instability, Journal of Computers and Physics, Vol. 152, No. 2, p. 642-663, 1999.

Huang, H., Thorne, D. T., Jr., Schaap, M. G., and Sukop, M. C., Proposed Approximation for Contact Angles in Shan-and-Chen-Type Multicomponent Multiphase Lattice Boltzmann Models, Physical Review E, Vol. 76, p. 66701-66706, 2007.

Huang, H., Li, Z., Liu, S., and Lu, X., Shan -and-Chen-type Multiphase Lattice Boltzmann Study of Viscous Coupling Effects for Two-phase Flow in Porous Media, Int. J. Numer. Meth. Fluids, Vol. 61, No. 3, p. 341-354, 2009.

Huang, H., and Lu, X., Relative Permeabilities and Coupling Effects in Steady-state Gas-liquid Flow in Porous Media: A Lattice Boltzmann Study, Physics of Fluids, Vol. 21, p. 92104-92112, 2009.

Huang, H., Wang, L., and Lu, X., Evaluation of Three Lattice Boltzmann Models for Multiphase Flows in Porous Media, Computers and Mathematics with Applications, Vol. 61, p. 3606-3617, 2011.

Kaviany, M., Principles of Heat Transfer in Porous Media, Springer, New York, 1995.

Lee, T., and Lin, C. L., Journal of Computers and Physics, Vol. 206, p. 16-47, 2005.

Li, H., Pan, C., and Miller, C. T., Pore-scale Investigation of Viscous Coupling Effects for Two-phase Flow in Porous Media, Physical Review , Vol. E72, p. 26705-26719, 2005.

Mohammad, A. A., and Kuzmin, A, A Critical Evaluation of Force Term in Lattice Boltzmann Method, Natural Convection Problem, International Journal of Heat and Mass Transfer Vol. 53, p. 990-996, 2010.

Pan, C., Hilpert, M., and Miller, C. T., Water Resources Research, Vol. 40, p. 1501-1508, 2004.

Rothman, D. H., and Keller, J. M., Immiscible Cellular-automaton Fluids, Journal of Statistical Physics, Vol. 52, p. 1119-1127, 1988.

Shan, X., and Chen, H., Lattice Boltzmann Model for Simulating Flows with Multiple Phases and Components, Physical Review E, Vol. 47, No. 3, p. 1815-1819, 1993.

Shan, X., and Doolen, G., Diffusion in a Multi Component Lattice Boltzmann Equation Mode, Physical Review E, Vol. 54, p. 3616-3620, 1996.

Sukop, M. C., and Or, D., Lattice Boltzmann Method for Modeling Liquid-vapor Interface Configurations in Porous Media, Water Resources Research, Vol. 40, p. 1509-1514, 2004.

Sukop, M., and Thorne, D., Lattice Boltzmann Modeling: an Introduction for Geoscientists and Engineers, New York, Springer, 172 p., 2007.

Swift, M. R., Osborn, W. R., and Yeomans, J. M., Lattice Boltzmann Simulation of Non-ideal Fluids, Physical Review Letters, Vol. 75, p. 830-833, 1995.

Yiotis, A. G., Psihogios J., and Kainourgiakis, M. E., A lattice Boltzmann Study of Viscous Coupling Effects in Immiscible Two-phase Flow in Porous Media, Colloids and Surfaces A, Physicochem. Eng. Aspects, Vol. 300, p. 35-49, 2007.